A numerical study of the general Rayleigh's piston model

1981 J. Phys. A: Math. Gen. 14 423

(http://iopscience.iop.org/0305-4470/14/2/018)

J. Phys. A: Math. Gen. **14** (1981) 423–438. Printed in Great Britain

A numerical study of the general Rayleigh's piston model

J Andrew Barker, M R Hoare and S Raval

Department of Physics, Bedford College, Regent's Park, London NW1 4NS, UK

Received 17 March 1980, in final form 3 July 1980

Abstract. We describe a detailed numerical investigation of the spectrum $\{\lambda_k, \lambda\}$ of the Rayleigh singular integral operator $\mathscr{A}_\gamma$ governing the one-dimensional test-particle gas at mass ratio γ (Rayleigh's piston). Results confirm that the discrete spectrum $\lambda_k(\gamma)$ is empty apart from the equilibrium eigenvalue, $\lambda_0 = 0$, in the range $\gamma > 0{\cdot}28\ldots$, but acquires new points in a regular manner as γ decreases. Thus the discretum interval $\lambda_k \in [0, 1]$ is gradually filled to ever-increasing density as the Brownian motion regime $\gamma \ll 1$ is reached. Spectra and eigenfunctions, together with derived results for the velocity autocorrelation function and complex admittance for charged test particles, are used to illustrate the effectiveness of the Rayleigh–Fokker–Planck approximation based on the artificial assumption $\gamma \to 0$.

1. Introduction

The general Rayleigh problem (or one-dimensional test-particle gas) may justly be described as the prototype for all linear statistical-dynamic models which retain at least a vestige of geometrical and mechanical reality (Rayleigh 1891, Hoare and Rahman 1973 and references therein). We refer here to the unsimplified case in which an ensemble of test particles of mass M undergoes interaction with a one-dimensional heat bath of particles of mass m and at temperature T, reserving the term *special* Rayleigh problem for the case $m = M$ to which we have devoted most of our attention so far (Hoare and Rahman 1973, 1974, 1976, Barker *et al* 1977, Raval 1978). The mass ratio $\gamma = m/M$ is thus of primary interest (figure 1).

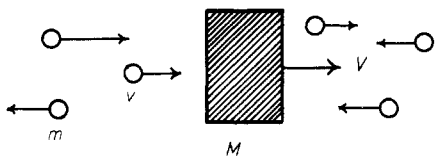

Figure 1. The Rayleigh piston. A piston of mass M and cross section σ undergoes random collisions with a one-dimensional heat bath of particles, mass m. The velocities of the heat bath particles are Maxwell distributed at temperature T and their number density is n per unit volume. $\gamma = m/M$.

Mathematically, the Rayleigh problem is defined by the singular Master equation

$$\frac{\partial P(x, t)}{\partial t} = \mathscr{A}_\gamma P(x, t) = \int_{-\infty}^{\infty} A(y, x) P(y, t)\, \mathrm{d}y \tag{1.1}$$

0305-4470/81/020423+16$01.50

in which $P(x, t)$ is the probability density for test particles at velocity x and $\mathscr{A}_\gamma$ is a singular integral operator having the kernel

$$A(y, x) = K(y, x) - z(x)\delta(x - y) \tag{1.2}$$

with

$$K(y, x) = \mu^2 |x - y| \exp\{-[(y - x)\mu + x]^2\} \tag{1.3}$$

and

$$z(x) = \int_{-\infty}^{\infty} K(x, y)\, dy = \exp(-x^2) + \pi^{1/2} x \operatorname{erf}(x). \tag{1.4}$$

Here μ relates to the mass ratio as $\mu = (1+\gamma)/2\gamma$ and x and y are scaled to real velocities V and V' as $x = (m/2k_B T)^{1/2} V$ and $y = (m/2k_B T)^{1/2} V'$. As in earlier work we use the time scale $\tau = n\sigma(2k_B T/\pi m)^{1/2} t$ with n and σ the effective number density and cross section of test particles respectively. The kernel $K(x, y)$ is referred to as the transition kernel for scattering $x \to dy$ about y and its integral $z(x)$, which rises monotonically from a minimum at $z(0) = 1$, represents the collision rate per scaled time for a test particle moving with velocity x. Here we may note that, in the present scaling, the equilibrium distribution of test particles becomes

$$P(x, \infty) = (\pi\gamma)^{-1/2} \exp(-x^2/\gamma) \tag{1.5}$$

which may easily be shown to satisfy $\mathscr{A}_\gamma P(x, \infty) = 0$.

As a final preliminary we may note the mean equilibrium collision number for test particles

$$\bar{z}_\infty = 2\int_0^{\infty} z(x) P(x, \infty)\, dx = 2(1+\gamma)^{1/2}. \tag{1.6}$$

This may be used to define an alternative time scale $\tau' = 2(1+\gamma)^{1/2}\tau$. The difference between the two scales is relatively minor in the interesting range of mass ratio $\gamma \in (0, 1)$.

With the exception of the two special cases $\gamma = 1$ and $\gamma \to 0$, very little is known about the form of solutions to (1.1) or the underlying spectral properties of the operator $\mathscr{A}_\gamma$. All we can say with certainty is that the singular character of $\mathscr{A}_\gamma$ manifests itself in a continuum spectrum $\lambda \in [1, \infty]$ to which a discretum $\lambda_k \in [0, 1]$ is added in a certain interval of γ. As the mass ratio is varied, the discretum is believed to consist of a finite set of eigenvalues: $1 > \lambda_{\max} > \ldots > \lambda_2 > \lambda_1 > \lambda_0 = 0$, which becomes empty except for the isolated equilibrium eigenvalue $\lambda_0 = 0$ above a certain threshold $\gamma > \gamma_0$ for which $\lambda_1(\gamma_0) \to 1$. The emptiness of the finite discretum $\lambda \in (0, 1]$ was demonstrated for the particular case $\gamma = 1$ (the special Rayleigh problem) by Hoare and Rahman (1973) but the presence of a finite empty region for $\gamma > \gamma_0$ as well as the non-existence of an infinite discretum with point of accumulation was a matter of conjecture, until recently proved by Driessler (1980). In singular stochastic problems of this kind, the finiteness of the discretum is by no means to be taken for granted; indeed in the case of the three-dimensional hard-sphere gas (about which, incidentally, rather more is known than for one dimension) there is an infinite discretum at all mass ratios with a point of accumulation at the continuum threshold $\lambda = \lambda^* = 1$. (See e.g. Hoare 1971, Hoare and Kaplinsky 1975, Shizgal 1979.) The distinctions between these types of spectra are made clear in figure 2.

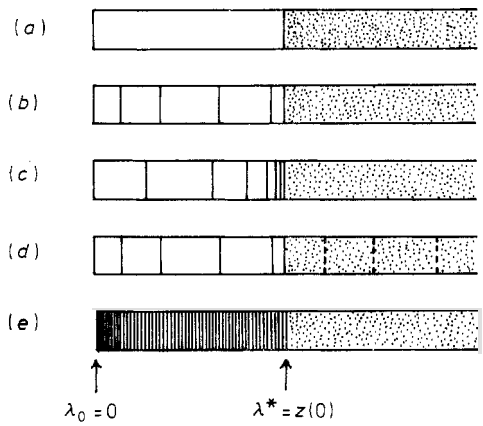

Figure 2. Possible types of spectra for the Rayleigh transition operator $\mathscr{A}_\gamma$. (*a*) Discretum empty for $\lambda \in (0, z(0))$. (*b*) Finite discretum $0 = \lambda_0 < \lambda_1 \ldots < \lambda_k < z(0)$. (*c*) Infinite discretum with point of accumulation such that $\lambda_k \to z(0)$ as $k \to \infty$. (*d*) Numerical approximate spectrum with converged discretum and 'pseudo-eigenvalues' $\lambda_k > z(0)$. (*e*) Spectrum for system approaching the Brownian motion limit with $\gamma \ll 1$. The continuum $\lambda \in (z(0), \infty)$ and the equilibrium eigenvalue $\lambda_0 = 0$ are always present.

There remains the somewhat insecure knowledge of the limit $\gamma \to 0$ in which the behaviour of the test particles assumes the character of Brownian motion. Since Rayleigh many authors have studied this approximation, both as a form of idealised limit and a supposedly useful description of systems at small but finite mass ratio (Van Kampen 1955, 1961, Akama and Siegel 1965a, b). The difficulties of this approach are well known and need not concern us in detail here. It may, however, be asserted with some confidence that in the passage to the limit $\gamma \to 0$ the discrete spectrum $\lambda_k(\gamma)$ becomes infinitely dense over the interval $\lambda_k \in [0, 1]$ and may, by a further time scaling $\tau^R = \tau/4\gamma^{1/2}$, be mapped onto the integers $\lambda_k^R = k + 1$ (Hoare and Rahman 1973).

While it is tempting to search for an exact solution to equation (1.1) along the lines successful in the case of $\gamma = 1$ (Barker *et al* 1977, Raval 1978), nothing in the character of the operator $\mathscr{A}_\gamma$ or its three-dimensional analogue lends much hope to this enterprise and our efforts in this direction have led to little worth reporting.

The time would therefore seem to have come for a thorough numerical study of the operator $\mathscr{A}_\gamma$ which might shed light on its spectral characteristics and put our knowledge in this respect on a similar footing to that available for some time in the three-dimensional case† (Hoare and Kaplinsky 1975). More broadly, we might define our objectives as follows:

† A number of comments are in order. The computations on the three-dimensional hard-sphere gas refer to the Wigner–Wilkins kernel for the half-range problem of *energy* relaxation with a kernel of type $K(x^2, y^2)$, $x, y \in (0, \infty)$ (Wigner and Wilkins 1944, Andersen and Shuler 1964). Thus a proper comparison would be with the half-range one-dimensional problem of either energy relaxation ($K(x^2, y^2)$) or speed relaxation ($K(|x|, |y|)$). However the speed kernel is simply the *even* component of the Rayleigh kernel (1.3) and its spectrum consists of the even subset of the full-range spectrum $\{\lambda_k\}$. (Actually $k = 0, 2, 4, \ldots$, as we may deduce from the parity of the Hermite polynomials and the fact that the spectrum curves $\lambda_k(\gamma)$ cannot cross.) With this in mind, a qualitative comparison of one- and three-dimensional models is possible. We note in passing that no kernel is available for the study of two-dimensional (hard-disc) scattering. Likewise, no spectral computations have been attempted on the full three-dimensional vector kernel $K(\boldsymbol{x}, \boldsymbol{y})$. (Nielsen and Bak 1964).

(a) To determine the behaviour of the discrete spectrum $\{\lambda_k(\gamma)\}$ of the operator $\mathscr{A}_\gamma$ over as large a range of mass ratio as possible, paying special attention to the finiteness or otherwise of the discretum and the behaviour of discrete relaxation modes in the immediate neighbourhood of the discretum.

(b) To compare, at least qualitatively, the spectra for one- and three-dimensional hard scattering.

(c) To assess the relative contributions of discretum and continuum to the evolution of the system, its equilibrium fluctuations and related transport properties.

(d) To investigate the effectiveness of the Fokker–Planck approximation to $\mathscr{A}_\gamma$ and its spectrum in the region $\gamma \ll 1$ and of possible improvements on this.

Bearing in mind the enormous literature on the Fokker–Planck equation and related aspects of Brownian motion, and the extreme rarity of cases where any kind of measure of the approximation against numerically soluble models is available, item (d) alone might almost be considered a principal justification for this paper.

2. Qualitative properties of the kernel

As a first step we prepared a series of graphical displays of the regular part $K(y, x)$ of the transition operator. These figures were of considerable help in planning detailed computations and their study gives a number of insights into the relaxation behaviour at different mass ratios. Two of them are shown in figure 3 for mass ratios $\gamma = 1.0$ and 0.5 respectively. Comparison of the figures shows the beginning of the tendency whereby the symmetric peaks narrow and encroach upon the diagonal as the Brownian motion limit $\gamma \to 0$ proceeds. The discontinuity of the first derivative at the diagonal $x = y$ is also clearly apparent. We need hardly point out that the vanishing of $K(x, y)$ at the diagonal, which is a consequence of the $|x - y|$ factor, has no analogue in the three-dimensional hard-sphere case of the *speed* or *energy* kernel (Wigner–Wilkins kernel) which we studied previously. A plot of the collision number function $z(x)$ is also given (figure 4). This shows $z(x)$ to be very close to its asymptotic form $z(x) \sim \pi^{1/2}x$ for $x > \sim 1{\cdot}5$, corresponding physically to the condition where the heat-bath particles are effectively stationary with respect to the moving test particle.

3. Analytical prerequisites

We may refer to Hoare (1971) for a detailed account of equation (1.1), its solutions and their approximations. Here we confine ourselves to a brief statement of the spectral form of the solution and its relation to our present numerical algorithm.

The time evolution of the probability density $P(x, \tau)$ under the operator $\mathscr{A}_\gamma$ may most conveniently be written

$$P(x, \tau) = P(x, \infty) + P(x, \infty)^{1/2}\mathbf{S}_{\lambda\in(0,\infty]}a(\lambda)N(x, \lambda)\exp(-\lambda\tau) \tag{3.1}$$

using the symbol S to indicate summation or integration, as appropriate, over the range shown in the subscript, and denoting by $N(x, \lambda)$ the eigenfunctions of the self-adjoint operator

$$\mathscr{B}_\gamma \equiv G(x, y) + z(x)\delta(x - y)$$

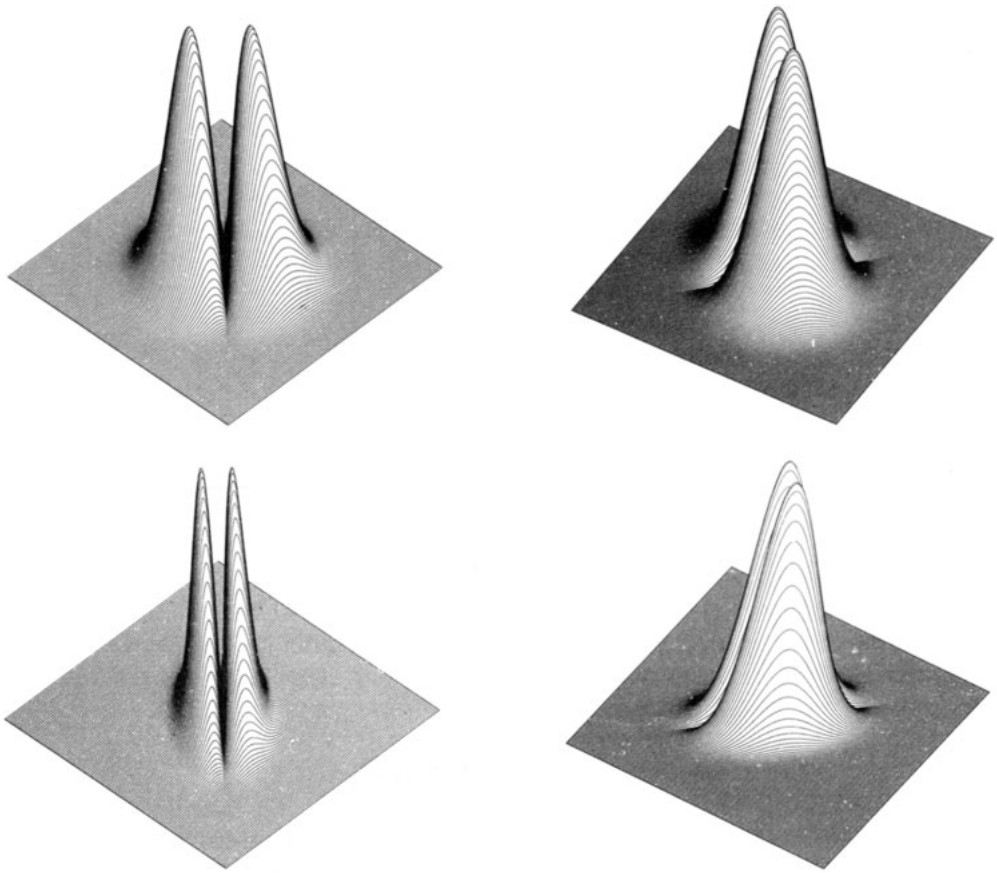

Figure 3. The symmetrised Rayleigh transition operator $G(x, y)$ (equation (3.3)). Above $\gamma = 1{\cdot}0$. Below $\gamma = 0{\cdot}5$. The coordinate origin is at the centre of the figure in each case, the diagonal $x = y$ running between the peaks. Note the discontinuity of the first derivative along this line.

the regular part of whose kernel is related to $K(x, y)$ by the similarity transformation

$$G(x, y) = K(x, y)[P(x, \infty)/P(y, \infty)]^{1/2} = G(y, x). \tag{3.2}$$

Substituting from (1.5) we obtain after slight rearrangement

$$G(x, y) = \mu^2|x - y| \exp[-\tfrac{1}{2}(x^2 + y^2) - \mu(\mu - 1)(x - y)^2]. \tag{3.3}$$

The symmetry of G is assured by the detailed balance property

$$P(x, \infty)K(x, y) = P(y, \infty)K(y, x) \tag{3.4}$$

as is the equilibrium condition

$$z(x)P(x, \infty) = \int_{-\infty}^{\infty} K(y, x)P(y, \infty)\,dy \tag{3.5}$$

with $P(x, \infty)$ given by equation (1.5).

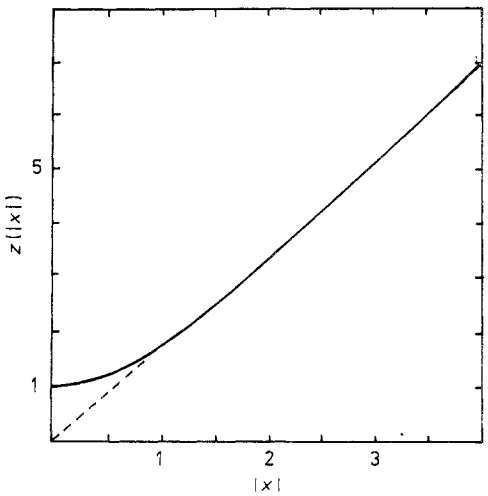

Figure 4. The collision number function $z(x) = \exp(-x^2) + \pi^{1/2}\,\mathrm{erf}(x)$ for Rayleigh test particles. The asymptote $z(x) \sim \pi^{1/2}x$ is shown dotted.

Since the spectrum is invariant under the transformation (3.2) while the singular component of $\mathscr{A}_\gamma$ is diagonal, it is obviously to our advantage to work with the symmetric eigenvalue equation

$$[z(x)+\lambda]\Phi(x,\lambda) = \int_{-\infty}^{\infty} G(x,y)\Phi(y,\lambda)\,\mathrm{d}y \tag{3.6}$$

or, as it is more natural to write when the discrete part of the spectrum is of interest:

$$[z(x)+\lambda_k]\Phi_k(x) = \int_{-\infty}^{\infty} G(x,y)\Phi_k(y)\,\mathrm{d}y. \tag{3.7}$$

It will be seen that, on choosing the appropriate normalisation, we can express the equilibrium condition by $\lambda_0 = 0$ and $\Phi_0(x)^2 = P(x,\infty) = (\pi\gamma)^{-1}\exp(-x^2/\gamma)$. With this in mind we have separated the $\lambda_0 = 0$ point on the right of equation (3.1) to leave a purely transient term under the S symbol.

In this paper our main attention goes to the solution of equations (3.6) or (3.7) using a simple discretisation method. We now turn to the details of this.

4. Description of the method

In our earlier study of the three-dimensional hard-sphere gas (Hoare and Kaplinsky 1975) we used a Rayleigh–Ritz method for the reduction of the eigenvalue problem $\mathscr{B}_\gamma\Phi = \lambda\Phi$ to an algebraic one. The polynomial set chosen as basis was that of the Laguerre polynomials $\{L_k^{(1/2)}(x)\}$ which are known to be exact left eigenfunctions of the transition operator in the Brownian limit $\gamma \to 0$. Although the Rayleigh–Ritz method is theoretically to be preferred because an $N \times N$ approximation may be refined without recalculation of the previous expansion matrix, in practice this is a slender advantage and the alternative of using a simple discretisation of the integral eigenvalue equation is neither difficult nor particularly wasteful of computing time. A proper discretisation

may indeed be somewhat more efficient than a RR method in as much as the discretised kernel remains strictly positive and the negative-going regions associated with polynomial expansions are avoided. A similar approach has been used for neutron thermalisation calculations in three dimensions (Wood 1965).

Thus we replace equations (3.6) and (3.7) by a comparable discretised form

$$[z_i - \lambda]\Phi_i(\lambda) = \sum_{j=1}^{N} G_{ji}\Phi_j(\lambda) \tag{4.1}$$

which has the matrix equivalent

$$[\mathbf{Z} - \lambda \mathbf{I}]\mathbf{\Phi} = \mathbf{G}\mathbf{\Phi}. \tag{4.2}$$

Having fixed N, the matrix elements G_{ij} are determined at the meshpoints as $G_{ij} = G(ih, jh)$ with the given mesh interval h. As will be clear on studying the graphical representations in figure 3, the choice of h and N must be made with some care.

We did not determine the diagonal matrix $\mathbf{Z}$ by discretisation of the collision number function $z(x)$ but instead generated it self-consistently in such a way as to conserve probability. Thus, using the transformation (3.2) with the discretised equilibrium distribution (1.5), we see that the required value is

$$z_i = h \exp[(ih)^2/2\gamma] \sum_{j=1}^{N} G_{ij} \exp[-(jh)^2/2\gamma]. \tag{4.3}$$

In this way the eigenvalue $\lambda_0 = 0$ is guaranteed.

The correspondence between an approximate spectrum $\{\hat{\lambda}_k\}$, obtained by solution of equation (4.2)—which is necessarily discrete—and the true spectrum $\{\lambda_k, \lambda\}$ has been discussed in detail by Hoare (1971). Briefly we may say that, as with quantum mechanical systems, a 'target' eigenvalue λ_k in the discretum is well approximated by taking a sufficiently detailed representation of the operator, provided that it lies well clear of the continuum threshold λ^*. (By 'representation' we mean either a Fourier expansion in basis functions or equally a discretisation seen as an approximation in step functions.) In this case a sequence of approximate eigenvalues $\hat{\lambda}_k$ will be found to converge more or less rapidly to the true value: $\hat{\lambda}_k \to \lambda_k$. If, however, the 'target' eigenvalue is near the continuum, poor numerical convergence will be found, with the approximate $\hat{\lambda}_k$ moving down through the latter towards the 'true' value. If a very detailed representation is attempted where there are few or even no discrete eigenvalues, then a non-convergent 'spread' of approximate $\hat{\lambda}_k$ will be found, many of which will be unrelated to any given discrete λ_k and yet, to an unknown degree of approximation, may be expected to 'represent' the continuum contribution to the action of the evolution operator $\mathscr{A}_\gamma$ (figure 2(*d*)). An extended account of the properties of the numerical $\hat{\lambda}_k$, including the 'pseudo-eigenvalues' $\hat{\lambda}_k > 1$ located in the continuum, will be found in Hoare (1971) and Hoare and Kaplinsky (1975). They need be of no further concern to us in this paper.

Finally we should recall that, with the continuum bounded below at $\lambda^* = 1$, any errors due to its neglect or faulty approximation will, *so long as a discrete spectrum actually exists*, only affect the time evolution appreciably in the regime $t < \sim z(0)^{-1}$, that is $\tau < \sim 1$. When the discretum is empty, as we know to be the case for $\gamma = 1$, the situation is clearly more complicated, though we can see that the modes close to the continuum threshold will tend to dominate increasingly as the system ages.

5. Computational procedures

Our main computational exercise was to determine eigenvalues and eigenvectors of the symmetric matrix $[\mathbf{G}-\mathbf{Z}]$ for a representative range of mass ratios in the range $\gamma < 1$. The subroutines used were from the NAG library and were run on the University of London CDC 7600 computer. Matrices up to 400×400 could be handled, though in almost all cases a 200×200 discretisation proved sufficient for our purpose. In practice preliminary runs were made using a 50×50 discretisation to determine the cutoff to the kernel $G(x, y)$ using a criterion that the determined eigenvector components at the boundary meshpoints should be no more than 10^{-3} of the maximum components. Having assigned a cutoff in this way, accurate computations were performed at each mass ratio with increasing values of N as a check on convergence. We were somewhat surprised to find that, even in the case of eigenvalues very close to the continuum, convergence was never a serious problem and all figures quoted in the tabulations in § 6 are significant. In scanning the range of mass ratios a preliminary tabulation was carried out for $\gamma = 2^{-k}$, $k = 0(1)7$. Intermediate values were then computed to establish the behaviour of the first few eigenvalues close to the continuum and interpolations were made as required for graphical presentation of the eigenvalues.

As the massive amount of data on approximate eigenvector components was of little use as it stood, we converted it to a much lower-order Fourier–Hermite representation. Our use of the basis functions $\{\phi_k\}$ for this purpose was partly a matter of convenience, but also in the knowledge that the 'pure' Hermite functions $\{\exp(-x^2/\gamma)H_k(x/\gamma^{1/2})\}$ are the natural choice for a function set complete and orthogonal with respect to the Maxwellian as weight function, as well as forming, incidentally, the exact eigenfunctions of the 'Fokker–Planck' operator $\mathscr{R}_\gamma$ which we introduce in the next section.

There is reason to hope that the Fourier–Hermite representation may be 'nearly diagonal' over an altogether broader regime of mass ratio, possibly even, as some authors have implied, in the vicinity of $\gamma = 1$. However, in contrast to Rayleigh–Ritz methods which provide Fourier coefficients directly, use of a discretisation requires that we extract them by carrying out a Fourier–Hermite transformation of the 'raw' eigenvectors of the matrix $\mathbf{G}-\mathbf{Z}$. This presented no difficulty and was carried out by use of Simpson's rule on the eigenvector components weighted by Hermite functions on the same discretisation grid.

As a preliminary to our calculations, we made a few determinations of eigenvalues and eigenvector components for the hard-sphere gas, comparing the discretisation results with the Rayleigh–Ritz ones of Hoare and Kaplinsky (1975). Over a series of spot checks, agreement was of the order of 5%.

6. Results and interpretation

6.1. The eigenvalue spectrum

The essential content of our results is seen most strikingly in the families of discrete eigenvalues plotted as a function of mass ratio in figure 5. The pattern indeed confirms the qualitative behaviour predicted earlier wherein the discrete eigenvalues emerge successively from the continuum and converge ever more densely into the interval $[0, 1]$ as the mass ratio tends to zero. Notably, not a single eigenvalue could be found to emerge from the continuum until the point $\gamma \simeq 0{\cdot}28$; moreover the presence of the

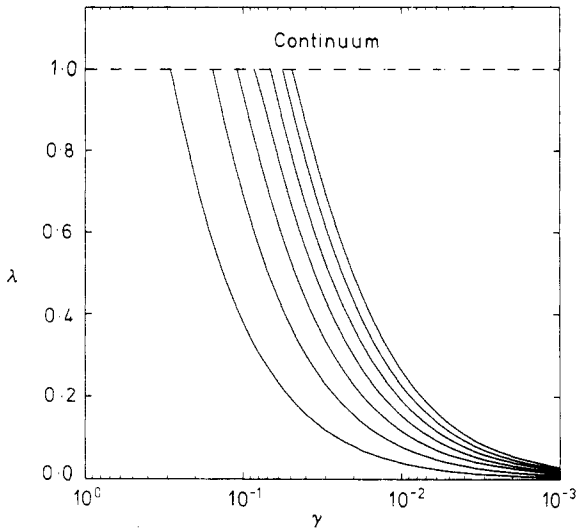

Figure 5. Numerical eigenvalues λ of the Rayleigh transition kernel (equations (1.2) to (1.4)) as a function of mass ratio γ. The discretum is seen to be empty in the range approximately $\gamma > 0{\cdot}28$.

continuum threshold was faithfully reflected in the boundary between 'convergable' and 'non-convergable' $\hat{\lambda}_k$ as the mesh size for the discretisation was diminished. Although for clarity we have only shown the first seven curves, the pattern continues in the same manner with what seems to be a regular increase in the density of points in the unit interval. As far as can be determined, given the weak convergence of points very close to the continuum, the curves $\lambda_k(\gamma)$ emerge at an appreciable angle to the continuum edge, there being no indication of a tangential flattening to a point of accumulation, such as is found in the three-dimensional case. We have not shown the continuation of the discrete λ_k into 'pseudo-eigenvalues' within the continuum since the position of these is a function of the mesh size and has no absolute importance. Nevertheless, it may be observed that, for N sufficiently high to give convergence of the discretum, the non-converged extensions of the curves shown were smooth extrapolations of negative slope, which showed no tendency to return to the discrete interval on increasing the mass ratio into the Lorentz region $\gamma \geqslant 1$. This confirms, so far as a numerical computation can, that the discretum indeed remains empty as the mass of the heat-bath particle increases to infinity. A few numerical values of the discrete λ_k are tabulated along with the eigenvector components in tables $1(a)$ to (f). These are scaled as $\lambda_k/4\gamma$ for reasons which will be evident in the next section.

6.2. Eigenvectors and the Fokker–Planck equation

It is widely believed that in the regime $\gamma \ll 1$ the effect of the operator $\mathscr{A}_\gamma$ may, under certain conditions on $P(x, \tau)$, be reproduced by the differential operator

$$\mathscr{R}_\gamma \equiv \frac{\gamma}{2}\frac{\partial^2}{\partial x^2} + x\frac{\partial}{\partial x} + 1 \tag{6.1}$$

together with a rescaling of the time in terms of the mass ratio. Thus if $\tau_R = 4\gamma\tau$ we find

Table 1. Rayleigh piston eigenfunctions in the Fourier–Hermite representation. Each column gives the expansion coefficients α_{ik} for the eigenfunction $N_i(x)$ in terms of the set $\{\exp(-x^2/\gamma)H_k(x/\gamma^{1/2})\}$ which are exact in the limit $\gamma \to 0$. All figures shown are significant. Asterisks indicate values absorbed into the continuum. The diagonal elements are in bold face. The $i = 0$ eigenfunction, for which necessarily $\alpha_{ik} = \delta_{k0}$, is shown as a check on numerical accuracy.

(*a*) $\gamma = 2^{-2}$									
$\lambda_i^R =$	0·00000	0·89239	*	*	*	*	*	*	*
k	$i=0$	1	2	3	4	5	6	7	8
0	**1·00000**	0·00000	*	*	*	*	*	*	*
1	0·00000	**0·99562**	*	*	*	*	*	*	*
2	0·00000	0·00000	*	*	*	*	*	*	*
3	0·00000	−0·08959	*	*	*	*	*	*	*
4	0·00000	0·00001	*	*	*	*	*	*	*
5	0·00000	0·02397	*	*	*	*	*	*	*
6	−0·00002	0·00014	*	*	*	*	*	*	*
7	0·00000	−0·00988	*	*	*	*	*	*	*
8	−0·00005	0·00003	*	*	*	*	*	*	*
(*b*) $\gamma = 2^{-3}$									
$\lambda_i^R =$	0·00000	0·94139	1·66442	*	*	*	*	*	*
k	$i=0$	1	2	3	4	5	6	7	8
0	**0·99999**	0·00000	0·00000	*	*	*	*	*	*
1	0·00000	**0·99944**	0·00000	*	*	*	*	*	*
2	0·00000	0·00000	**0·99399**	*	*	*	*	*	*
3	0·00000	−0·03310	0·00000	*	*	*	*	*	*
4	0·00002	0·00000	−0·10748	*	*	*	*	*	*
5	0·00000	0·00346	0·00000	*	*	*	*	*	*
6	0·00000	0·00000	0·00002	*	*	*	*	*	*
7	0·00000	−0·00062	0·00003	*	*	*	*	*	*
8	0·00001	0·00001	−0·00548	*	*	*	*	*	*
(*c*) $\gamma = 2^{-4}$									
$\lambda_i^R =$	0·00000	0·96982	1·82346	2·57328	3·22952	3·80053	*	*	*
k	$i=0$	1	2	3	4	5	6	7	8
0	**0·99999**	0·00000	0·00000	0·00000	0·00000	0·00000	*	*	*
1	0·00000	**0·99989**	0·00000	0·01448	0·00000	0·00063	*	*	*
2	0·00000	0·00000	**0·99903**	0·00000	0·04370	0·00000	*	*	*
3	−0·00001	−0·01449	0·00001	**0·99568**	0·00000	0·09004	*	*	*
4	0·00000	0·00000	−0·04381	0·00009	**0·98586**	0·00004	*	*	*
5	0·00000	0·00063	0·00004	−0·09083	0·00044	**0·96149**	*	*	*
6	0·00001	0·00002	0·00307	0·00022	−0·15915	0·00157	*	*	*
7	0·00000	−0·00021	0·00012	0·00925	0·00077	−0·25255	*	*	*
8	0·00000	0·00005	−0·00120	0·00045	0·02209	0·00187	*	*	*
(*d*) $\gamma = 2^{-5}$									
$\lambda_i^R =$	0·00000	0·94632	1·83613	2·76440	3·46240	4·39497	4·90453	6·16978	6·87916
k	$i=0$	1	2	3	4	5	6	7	8
0	**0·99999**	0·00000	0·00000	0·00000	0·00003	0·00002	0·00000	0·00001	0·00000
1	0·00000	**0·99999**	0·00000	0·00000	0·00000	0·00000	0·00000	0·00000	0·00003
2	0·00000	0·00000	**0·99984**	0·00000	0·01896	0·00000	−0·00056	0·00001	0·00000
3	0·00000	−0·00650	0·00000	**0·99930**	0·00000	0·03785	0·00000	0·00178	0·00000
4	0·00000	0·00000	−0·01896	0·00000	**0·99777**	0·00000	0·06368	0·00007	0·00006
5	0·00000	0·00014	0·00000	−0·03786	−0·00001	**0·99457**	0·00000	−0·09632	0·00000
6	0·00000	0·00000	0·00064	0·00000	−0·06375	0·00010	**0·98791**	−0·13789	−0·00025
7	0·00000	0·00000	0·00000	0·00187	−0·00004	−0·09736	0·00004	**0·97564**	−0·00001
8	0·00000	0·00000	−0·00006	0·00002	0·00426	0·00020	−0·13989	0·00165	**0·95335**

Table 1—continued

(*e*) $\gamma = 2^{-6}$								
$\lambda_i^R =$	0·00000	0·99245	1·95424	2·88640	3·79048	4·67028	5·53489	6·40040	7·28600
k	$i=0$	1	2	3	4	5	6	7	8
0	**0·99999**	0·00000	0·00011	0·00000	0·00000	0·00000	0·00000	0·00000	0·00000
1	0·00000	**0·99999**	0·00000	−0·00348	0·00000	−0·00002	0·00000	−0·00001	0·00000
2	−0·00011	0·00000	**0·99998**	0·00000	0·00974	0·00000	0·00015	0·00000	0·00003
3	0·00000	−0·00349	0·00000	**0·99995**	0·00006	0·01915	0·00008	0·00060	0·00003
4	0·00000	0·00000	0·00985	−0·00016	**0·99987**	0·00037	0·03258	0·00039	0·00248
5	0·00000	−0·00002	0·00006	0·01993	0·00092	**0·99970**	0·00151	0·05221	0·00124
6	−0·00001	0·00003	−0·00029	−0·00035	−0·03561	−0·00374	**0·99937**	−0·00409	0·08128
7	0·00000	−0·00018	0·00016	0·00203	0·00142	0·06736	0·01087	**0·99882**	0·00757
8	0·00004	0·00005	−0·00110	−0·00103	0·00067	−0·00876	0·00359	−0·12663	**0·99797**
(*f*) $\gamma = 2^{-7}$								
$\lambda_i^R =$	0·00000	0·99744	1·99739	2·94607	3·89775	4·83484	5·75852	6·67232	7·58478
k	$i=0$	1	2	3	4	5	6	7	8
0	**1·00000**	0·00000	0·00011	0·00000	0·00000	0·00000	0·00000	0·00000	0·00000
1	0·00000	**0·99999**	0·00000	0·00141	0·00000	0·00001	0·00000	0·00000	0·00000
2	0·00011	0·00000	**0·99999**	0·00000	0·00431	0·00000	0·00000	0·00002	0·00000
3	0·00000	−0·00141	0·00000	**0·99996**	0·00000	0·00861	0·00000	0·00009	0·00000
4	0·00000	0·00000	−0·00432	0·00000	**0·99987**	−0·00002	0·01438	−0·00003	0·00002
5	0·00000	0·00000	0·00001	−0·00863	0·00002	**0·99962**	−0·00015	0·02192	−0·00019
6	0·00000	0·00000	0·00002	0·00001	−0·01457	0·00030	**0·99882**	−0·00069	0·03220
7	0·00000	0·00000	0·00000	−0·00001	0·00011	−0·02285	0·00139	**0·99629**	−0·00233
8	0·00001	0·00000	−0·00005	0·00006	−0·00044	−0·00053	−0·03618	0·00479	**0·98876**

by arguments closely similar to those advanced by Rayleigh (1891) that

$$\partial P(x, \tau_R)/\partial t = \mathscr{R}_\gamma P(x, \tau_R) \tag{6.2}$$

replaces satisfactorily the singular Master equation (1.1). The operator $\mathscr{R}_\gamma$ has the complete set of eigenfunctions

$$\phi_k^R(x) = \exp(-x^2/\gamma) H_k(x/\gamma^{1/2}) \tag{6.3}$$

for which the eigenvalues are $\lambda_k = k$, $k = 0, 1, 2, \ldots \infty$. The right-hand side of equation (3.1) therefore becomes a simple summation. For the special case $P(x, 0) = \delta(x - x_0)$ this summation can be carried out in closed form (Mehler's formula). The result is Rayleigh's formula, which in our scaled variables reads

$$P(x, x_0, \tau_R) = \frac{1}{[\gamma\pi(1-\exp(-2\tau_R))]^{1/2}} \exp\left[\frac{-(x - x_0\exp(-\tau_R))^2}{\gamma(1-\exp(-2\tau_R))}\right]. \tag{6.4}$$

That this approximation covers a multitude of sins is well known, and we have previously stressed that, however small a value of γ may be taken, any notion of a true 'convergence' of $\mathscr{R}_\gamma$ to $\mathscr{A}_\gamma$ is illusory.

We see this most clearly in the fact that, in the τ_R time scale, the continuum threshold is displaced not to infinity but only to $\lambda = (4\gamma)^{-1}$ so that the (exact!) eigenvalues of the operator $\mathscr{R}_\gamma$ must lie within it for $k > \sim(4\gamma)^{-1}$. Our hopes that $\mathscr{R}_\gamma$ nevertheless provides a 'reasonable' approximation to $P(x, \tau)$ rest on the suppositions that (a) sufficient true, discrete eigenvalues λ_k actually exist and are well approximated by $\lambda_k^R = 4\gamma k$, that all Fourier–Hermite coefficients a_k of $P(x, \tau)$ outside the same range of k at time τ_R are negligible, and/or (b) the infinite ladder of eigenvalues $\lambda_k > (4\gamma)^{-1}$ is

sufficiently dense and otherwise matched to the continuum that the latter is in some sense also 'represented', and (c) the matching of approximate polynomial eigenfunctions to both regular and singular 'true' eigenfunctions is correspondingly adequate. (See Hoare and Kaplinsky (1975) for an elaboration of these conditions.)

While some estimate of the truth of proposition (b) may be possible by a form of continuum variation method applied to $\mathscr{A}_\gamma$, it is clear that the present computations can only help to shed light on proposition (a). As a first step we therefore rescale the spectra of figure 5 by $\lambda_k^R = \lambda_k/4\gamma$. This displaces the continuum and leads to the family of curves shown in figure 6. Here it can be seen at a glance that, provided the eigenvalues concerned are not too close to the continuum edge, the values of λ_k^R for small k are surprisingly well represented by the integers. While this approximation clearly deteriorates with increasing k it is remarkable that the lowest eigenvalue λ_1^R is quite close to unity (0·89 . . .) even at the point where it emerges from the continuum.

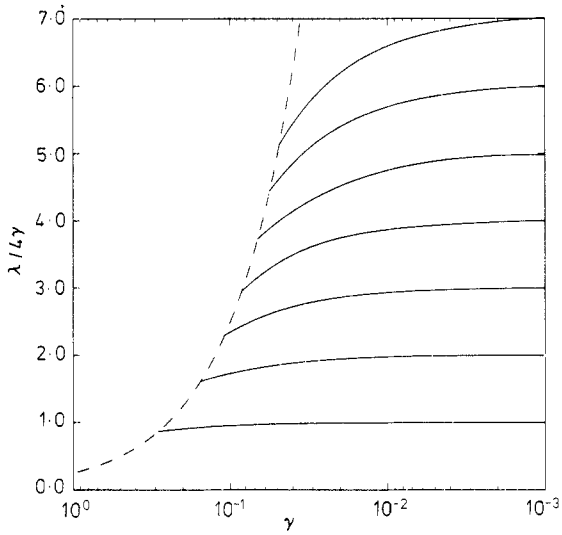

Figure 6. Eigenvalues of the Rayleigh kernel in the Fokker–Planck time scale $\tau^R = 4\gamma\tau$.

The same pattern is found when we investigate the eigenvectors in their Fourier–Hermite representation (tables 1(*a*) to (*f*)). Here we notice immediately the nearly diagonal aspect of the low-index part of these matrices even at mass ratios considerably higher than would normally be associated with Brownian motion. Reference to the corresponding tables for the three-dimensional case in Hoare and Kaplinsky (1975) shows that the off-diagonal contributions grow altogether more rapidly in the system of hard spheres. In short, the Fokker–Planck approximation appears to be appreciably better in one dimension than three, whether judged by the spectra λ_k or by the more sensitive eigenvectors.

Lastly we make brief mention of the 'improved' Fokker–Planck estimate proposed by Hoare and Rahman (1973). In this work an alternative infinite-order differential operator representation for $\mathscr{A}_\gamma$ was found which, when truncated at second order, seems likely to give improved estimates of the spectrum. The values obtained were

given by the equation†

$$\lambda_k = 4b^2\{(2k+1)[1+2b^2+b^4(2k+1)^2]^{1/2} - b^2(2k+1)^2 - 1\}$$
$$b^2 = \tfrac{1}{2}[\gamma/(1+\gamma)]. \tag{6.5}$$

This same expression could be used to predict the point of emergence of the first eigenvalue λ_1 from the continuum as $\gamma = [3(\sqrt{2}-1)]^{-1} = 0{\cdot}805\ldots$. This value could be construed as a bound to the region of emptiness of the discretum if certain positivity conditions were assumed. The present numerical results lend no support to the above expression as an accurate predictor of the spectrum.

6.3. Autocorrelation functions

In many respects the equilibrium fluctuations of a statistical model are of more interest than the computation of initial-value relaxation from an arbitrary distribution $P(x, 0)$. The scaled velocity autocorrelation function $S_x(\tau)$ takes a particularly simple form when expressed in terms of Fourier coefficients for an orthogonal polynomial representation (Hoare 1971, Raval 1978). We find that

$$S_x(\tau) = \sum_{k=1}^{N} [\alpha_1^{(k)}]^2 \exp(-\hat{\lambda}_k \tau) \tag{6.6}$$

where $\alpha_1^{(k)}$ is the first Fourier–Hermite coefficient of the kth eigenfunction. The summation may be taken over as many eigenvalues as are available including 'pseudo-eigenvalues' if desired. We included them here.

The results of this exercise can be seen in figure 7. While rather more detailed data would have been desirable at this point, we can perceive a relatively large alteration in the degree of persistence of velocity in passing from $\gamma = 1$ to $\gamma = \frac{1}{2}$ followed by a much more gradual shift over the range $\gamma = 2^{-2}$ to 2^{-7}. Although without a proper understanding of the effect of the continuum no definite explanation can be given, it seems reasonable to attribute this relatively sudden change in autocorrelation to the emergence of the first discrete eigenvalue λ_1 from the continuum and its subsequently rapid decay towards zero on the τ time scale as $\gamma \to 0$. By the time a mass ratio is reached where several eigenvalues might contribute to the transient $\exp(-\lambda_k \tau)$, the off-diagonal coefficients $\alpha_1^{(k)}$ have so decreased in magnitude that the result is virtually indistinguishable from the Gaussian limit: $S_x(\tau) = \frac{1}{2}\exp(-4\gamma\tau)$. When $S_x(\tau)$ is plotted logarithmically, a distinct curvature is seen for each mass ratio when $\tau < 0{\cdot}2$, this persisting to the region of $\tau < 1$ for the case $\gamma = 1$. Outside these regions the decay of correlations appears virtually exponential.

There is again a distinct difference between one- and three-dimensional behaviour, for in the latter a much more regular spread of the $S_x(\tau)$ curves results. However we must not make too much of this for it is clear that, whereas in one dimension persistence of velocity can only be governed by a discrepancy in mass, in three there is a strong geometrical component in the form of glancing collisions.

† The work of Hoare and Rahman (1973) is in error where these authors suggest that the above bound may be converted to a related one for a finite region of emptiness of the discretum in the Lorentz regime $\gamma > 1$. The whole question of the nature of the spectrum in the Lorentz regime would appear to us to remain open. Some progress in the rigorous study of these questions has been reported by W Driessler (private communication).

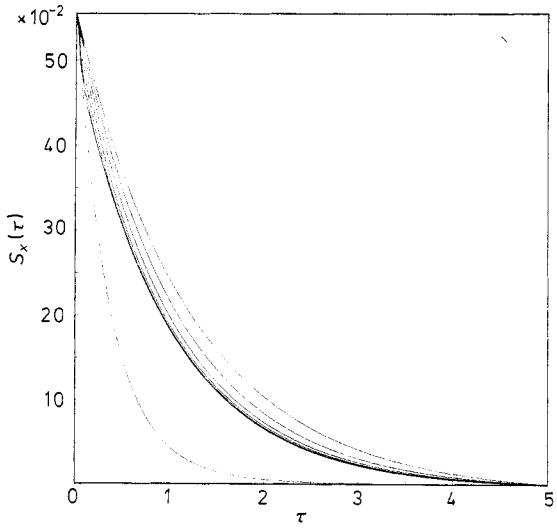

Figure 7. Velocity autocorrelation function, $S_x(\tau)$, for Rayleigh test particles as a function of mass ratio γ. The curves shown are for $\gamma = 1$ (lowest) to $\gamma = 2^{-7}$ (highest) in powers of 2. The lines for $\gamma = 2^{-2}$ to 2^{-4}, though distinct at short times, are virtually indistinguishable after $\tau = 0{\cdot}5$.

6.4. The complex admittance

A further property of considerable interest is the complex admittance, which contains all essential information about the response of an ideal ensemble of charged test particles to an applied AC field. Following Kubo (1957), the ratio of the admittance $\sigma(\omega)$ at frequency ω to the DC conductivity σ_0 at zero frequency can be expressed in the form

$$\left(\frac{\sigma(\omega)}{\sigma_0}\right) = \int_0^\infty \exp(i\omega\tau) S_x(\tau)\, d\tau \Big/ \int_0^\infty S_x(\tau)\, d\tau. \tag{6.7}$$

Note that the integral in the denominator is the scaled self-diffusion coefficient in the Kubo formulation.

Using again the Fourier–Hermite representation as in equation (6.6) we see that the admittance takes the form

$$\left(\frac{\sigma(\omega)}{\sigma_0}\right) \simeq \left(\sum_{k=1}^{N} [\alpha_1^{(k)}]^2/(\hat{\lambda}_k - i\omega)\right) \Big/ \left(\sum_{k=1}^{N} [\alpha_1^{(k)}]^2/\hat{\lambda}_k\right). \tag{6.8}$$

Three main quantities of interest can be extracted from the above formula: the conductivity $\mathrm{Re}(\sigma(\omega))$, which determines the dissipative flux of energy into the heat bath, $|\sigma(\omega)|$, the effective electrical impedance, and $\phi = \tan^{-1}[\mathrm{Im}(\sigma(\omega))/\mathrm{Re}(\sigma(\omega))]$ measuring the phase lag in the response of the test particles. The values of these quantities, computed according to equation (6.8), may be read from figure 8.

Again there is a relatively sudden shift in the position of the curves as the discrete eigenvalues begin to emerge from the continuum at a mass ratio of about 3 : 1, followed by a more gradual development towards a Lorentz type dependence in the Brownian motion limit. Not unexpectedly, the mean collision time for stationary particles

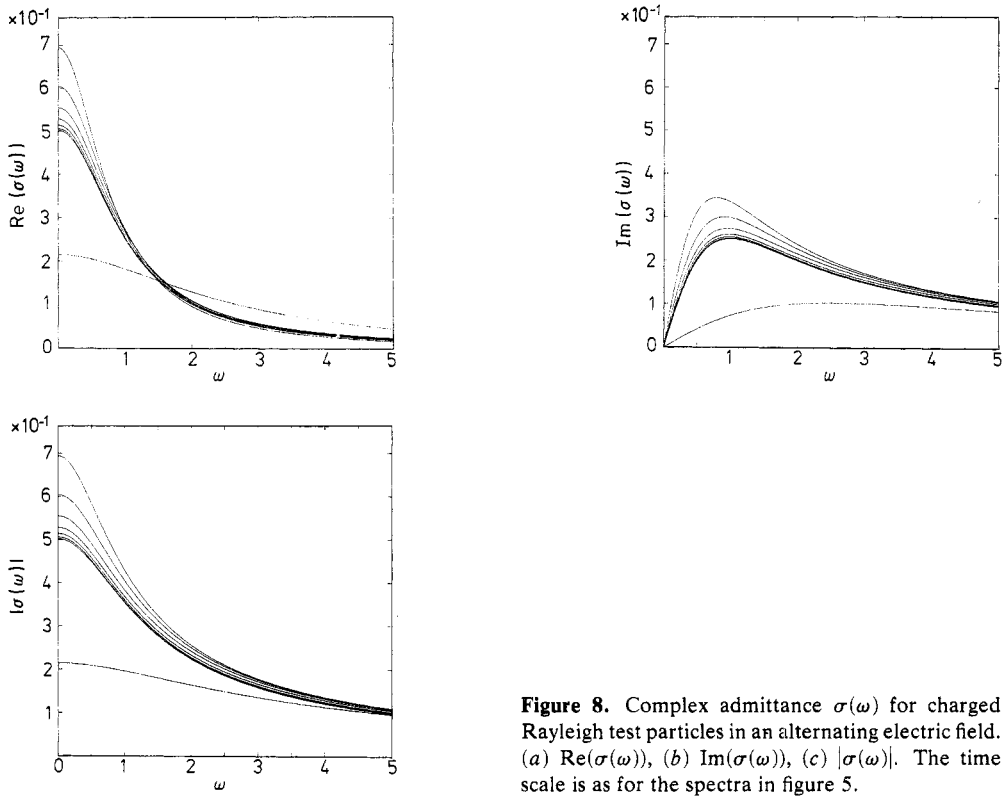

Figure 8. Complex admittance $\sigma(\omega)$ for charged Rayleigh test particles in an alternating electric field. (*a*) $\mathrm{Re}(\sigma(\omega))$, (*b*) $\mathrm{Im}(\sigma(\omega))$, (*c*) $|\sigma(\omega)|$. The time scale is as for the spectra in figure 5.

$\omega^{-1} = z(0)^{-1} = 1$ lies within the region of rapid change at low mass ratios, though a field frequency of many times the mean collision frequency is required to make the AC conductivity effectively zero.

7. Conclusion

With these results we may reasonably claim to have elucidated the eigenvalue properties of the simplest singular integral operator yet studied which has both clear dynamical interpretation and a non-trivial spectrum. The calculations make plain the nature of the passage to Brownian motion in a particular system while showing beyond doubt that in no approximation to its transition operator can we afford to neglect the continuum spectrum, especially as concerns the initial value problem at short times and moderate mass ratios. They also underline the remarkable qualitative change which may come about with the emergence of a first discrete eigenvalue from a continuum, a previously unsuspected result which may well have bearing on more complicated model systems.

As we earlier indicated, this type of computation could be extended to yield information about the continuum itself in terms of discrete 'pseudo-eigenvalues', which may provide the most accessible method of studying the onset of inverse Brownian motion in the 'Lorentz regime' as $\gamma \to \infty$. While certain tentative conclusions may be drawn, it is also clear that these require the suspension of doubt on a number of mathematical questions of a different order of complexity to those raised here. We have

therefore confined ourselves for the present to the discrete relaxation process. An extended account of the continuum for the special case $\gamma = 1$ is given by Raval (1978) and M R Hoare, M Rahman and S Raval, to be published.

References

Akama H and Siegel A 1965a *Physica* **31** 1493–519
—— 1965b *Phys. Fluids* **8** 1218–36
Andersen K and Shuler K E 1964 *J. Chem. Phys.* **40** 633–50
Barker J Andrew, Hoare M R, Rahman M and Raval S 1977 *Can. J. Phys.* **55** 916–28
Driessler W 1980 *Commun. Math. Phys.* (to appear)
Hoare M R 1971 *Adv. Chem. Phys.* **20** 135–214
Hoare M R and Kaplinsky C H 1975 *Physica* **81**A 349–68
Hoare M R and Rahman M 1973 *J. Phys. A: Math., Nucl. Gen.* **6** 1461–78
—— 1974 *J. Phys. A: Math., Nucl. Gen.* **7** 1070–93
—— 1976 *J. Phys. A: Math. Gen.* **9** 77–85
Kubo R 1957 *Proc. Phys. Soc. Jap.* **12** 570–86
Nielsen S E and Bak T A 1964 *J. Chem. Phys.* **41** 665–74
Raval S 1978 *PhD Thesis* University of London
Rayleigh (1st Baron) (Strutt J W) 1891 *Phil. Mag.* **32** 424–45 (See also 1902 *Collected papers* vol 3 (Cambridge: CUP) pp 473–85)
Shizgal B 1979 *J. Chem. Phys.* **70** 1948–51
Van Kampen N G 1955 *Physica* **21** 949–58
—— 1961 *Can. J. Phys.* **39** 551–67
Wigner E P and Wilkins J E 1944 *Atomic Energy Commission Report* D-2275
Wood T 1965 *Proc. Phys. Soc.* **85** 805–7